

Use of Iron Ore Tailing as Raw Material for Two Products: Sodium Silicate and Geopolymers

Caroline D. Prates,^a Athos S. Lima,^a Igor C. Ferreira,^b Fabiano G. F. de Paula,^a
Paula S. Pinto,^{a,c} José D. Ardisson,^d Rochel M. Lago^a and Ana Paula C. Teixeira^{✉*,a}

^aDepartamento de Química, Instituto de Ciências Exatas, Universidade Federal de Minas Gerais,
31270-901 Belo Horizonte-MG, Brazil

^bDepartamento de Engenharia de Minas, Universidade Federal de Minas Gerais,
31270-901 Belo Horizonte-MG, Brazil

^cDepartamento de Ciências Naturais e da Terra, Universidade do Estado de Minas Gerais (UEMG),
35501-170 Divinópolis-MG, Brazil

^dCentro de Microscopia da UFMG, Universidade Federal de Minas Gerais,
31270-901 Belo Horizonte-MG, Brazil

In this work, iron ore tailing (IOT) was used for the production of two different materials: sodium silicate and geopolymers. Initially, reactions of IOT with NaOH were carried out by hydrothermal reaction in autoclave at 200 °C (1:1.5 and 1:2.5 SiO₂:NaOH molar ratio) and reaction times of 4 and 8 h. X-ray fluorescence by dispersive energy (XRF), X-ray diffraction (XRD), Mössbauer spectroscopy, scanning electron microscopy (SEM-EDS) and titrations showed that IOT:NaOH ratios of 1:2.5 and reaction time 8 h completely dissolved the quartz from the IOT, obtaining a solid fraction consisting mainly of hematite and an aqueous phase of sodium silicate, which showed contents of ca. 23% SiO₂ and 19% Na₂O. This sodium silicate obtained was then combined with IOT (25 and 50 wt.%) to produce geopolymeric material with excellent physico-chemical properties, fast curing time and very good compressive strength results, which ranged from 41 to 58 MPa and many potential applications.

Keywords: iron ore tailing, geopolymer, sodium silicate

Introduction

The main mineral explored in Brazil is iron ore and mining companies generate a large amount of tailings due to their intense production. About 0.4 tons of tailings are produced for every 1 ton of iron ore processed.¹ In 2019, about 153.9 million tons of tailings were generated in Brazil.² In Minas Gerais state, dams, which have significant environmental impacts, characterize the main form of mining waste storage.³

In view of the great volume of mining tailings and the environmental impacts related to their storage, several studies have been carried out aiming the reuse of these wastes.⁴⁻⁶

Carmignano *et al.*⁵ published a review article in the year 2021, bringing a lot of information about tailings and their applications. Among these applications, we can

highlight the area of civil construction, ceramic industry and alkaline activated materials, in addition to other more technological applications, such as synthesis of zeolites, mesoporous silica, carbon nanotubes, adsorptions, catalysis and batteries.

In the iron ore beneficiation process, two types of tailings are produced: the mud, rich in iron, resulting from the desliming process, and the sandy tailings, a sand rich in quartz, resulting from the tailings flotation process.⁷

Among the various applications for iron-rich mud, we can mention: Prates *et al.*⁸ used the tailings from iron mining for the synthesis of a heterogeneous acid catalyst to produce biodiesel. Silva⁹ also used them as a catalyst, but for the production of carbon nanomaterials applied in the adsorption of contaminants, while Luciano *et al.*¹⁰ used the tailings as a source of iron to promote thermal decomposition of organic compounds to obtain biofuels.

As for the sandy tailings, rich in quartz, some examples of applications are in the replacement of sand for production

*e-mail: anapct@ufmg.br

Editor handled this article: Célia M. Ronconi (Associate)

of concrete and mortars, production of ceramics, synthesis of silicates and production of geopolymers.^{5,7,11,12}

Geopolymers can be defined as inorganic polymers obtained by the alkaline activation of aluminosilicates at low temperatures. They are constituted by a three-dimensional network in which the silicon atoms alternate with those of aluminum in tetrahedral coordination, sharing all the oxygen.¹³ Due to their characteristics, geopolymers have been applied in several types of industries. Its main application is in the area of civil engineering, replacing Portland cement, and has several advantages such as greater durability, greater mechanical resistance, lesser drying time, greater chemical stability, allowing perfect finishes, in addition to the production process emitting much less CO₂.^{14,15} In this way, the production of geopolymers can be an excellent alternative to transform iron mining tailings into high quality civil construction material.

Several studies have been carried out aiming at the use of tailings to produce geopolymers. The red mud, bauxite tailings generated in the Bayer aluminum production process, has a high alkalinity and a significant content of silicon and aluminum compounds. These characteristics make it an excellent raw material for the production of geopolymers, as has been verified in some studies.¹⁶⁻¹⁸ Tailings from iron beneficiation process have significant levels of silicon compounds and have also been studied as a raw material for geopolymers.¹⁹⁻²¹

Kuranchie *et al.*²¹ present a methodology for manufacturing geopolymer bricks using tailings from iron ore mines in Western Australia. In this study, a commercial sodium silicate solution was added to the tailings and various parameters were tested such as the effects of initial setting time, cure temperature, cure time and alkaline activator content. The bricks reached compressive strength values up to 50.53 MPa when cure temperature and cure time were 80 °C and 7 days. But for bricks cured at room temperature the mechanical strength values were very low (0.7 MPa).²¹

Sodium silicate is the main and most expensive raw material for geopolymers production. In addition, sodium silicate can also be produced from sandy tailings, due to the silica-rich composition of the tailing.⁷

The conventional process of producing sodium silicate is via calcination of a mixture of sodium carbonate (Na₂CO₃) and natural quartz sand (SiO₂) at 1400-1500 °C, leading to high energy consumption, maintenance cost and contaminant emission dust and CO₂.²² Therefore, the production of sodium silicate through alternative routes is of great importance. Among these alternative routes, it can be mentioned the production of sodium silicate by the reaction of SiO₂ with NaOH at high temperatures as described in some works and patents.²³⁻²⁷

Foletto *et al.*²² used rice husk ash to produce sodium silicate from a hydrothermal reaction in an autoclave with NaOH solutions with conversions of ca. 94% of the silica present in the rice husk ash into sodium silicate using a 2:1 molar fraction of NaOH:SiO₂ and a temperature of 200 °C. Vinai *et al.*²⁸ developed a simple process to produce sodium silicate powder from glass shell, which consisted of mixing the glass powder with sodium hydroxide and water, followed by a heating step at temperatures of 150 to 330 °C. Figueiredo *et al.*⁷ produced powdered sodium silicate by heating a mixture of iron mining waste, sodium hydroxide and water at 350 °C.

In this work, an iron ore tailing (IOT) was used to produce sodium silicate (unprecedented production via the hydrothermal route using IOT), which was applied as an alkaline activator solution for geopolymers synthesis. In addition, iron waste has also been tested as a filler in the production of geopolymers. Thus, in this work, for the first time, alternatives are suggested for two environmental problems simultaneously: the storage of mining tailings and the large emission of CO₂ generated in the production of Portland cement.

Experimental

Sodium silicate synthesis

The sandy tailings were obtained by Samarco (Mariana, Brazil) from iron ore beneficiation process. In a first step, we dried the IOT at 80 °C to obtain a fine dry powder.

Different mixtures were prepared containing samples of the tailings, sodium hydroxide (NaOH, Synth, Diadema, Brazil) and water, to get materials with molar ratios of 1:1.5 and 1:2.5 of Si:NaOH. The mixtures were placed in an autoclave and heated in a muffle furnace until 200 °C (heating rate of 10 °C min⁻¹) at 4 and 8 h. The liquid fraction was separated from the solid fraction by centrifugation and stored for further analysis. The solid products obtained were washed with water until neutral pH and dried in an oven at 80 °C for 24 h. The materials obtained were named according to the amount of NaOH used and the reaction time, as shown in Table 1.

Table 1. Materials nomenclature and main conditions of of the sodium silicate synthesis

| Nomenclature | Molar ratio Si:NaOH | Reaction time / h |
|--------------|---------------------|-------------------|
| T1.5-4 | 1:1.5 | 4 |
| T1.5-8 | 1:1.5 | 8 |
| T2.5-4 | 1:2.5 | 4 |
| T2.5-8 | 1:2.5 | 8 |

The IOT and the obtained solids were analyzed by different characterization techniques. The quantitative chemical composition of the iron tailings was determined by X-ray fluorescence by dispersive energy (XRF) in a Shimadzu EDX-720 spectrometer (Kyoto, Japan) under vacuum. The structural characterization was performed by X-ray powder diffraction (XRD) on a Shimadzu diffractometer, model XRD-7000 (Kyoto, Japan) with Cu K α radiation (1.5406 Å) and scanning speed of 4° min⁻¹. The ⁵⁷Fe Mössbauer spectra were obtained in a conventional spectrometer (CMTE model MA250, Starnberg, Germany) at room temperature on a constant acceleration transducer with a ⁵⁷Co/Rh source. The spectra were adjusted using a numerical program known as NORMOS.²⁹ Scanning electron microscopy (SEM) images were obtained on a FEI Quanta 3D microscope equipped with Bruker Silicon Drift Detector (Billerica, USA). For energy dispersive X-ray scattering (EDS) mappings 15 kV high voltage, 4.5 spot size and 50 µm objective aperture were used for good signal to noise ratio. The Na₂O and SiO₂ contents of the liquids obtained in the reactions were analyzed by volumetric titration with HCl.³⁰

Geopolymers synthesis

The raw materials used in the preparation of geopolymers are: iron ore tailing, sodium silicate (Sulfal Química, Belo Horizonte, Brazil), sodium hydroxide (Sulfal Química, Belo Horizonte, Brazil) and metakaolin (Metacaulim Brasil, Jundiaí, Brazil).

The production of geopolymers followed the procedures described by Ferreira *et al.*³¹ The standard alkaline activator was previously prepared from a 10 M sodium hydroxide solution and a sodium silicate solution (32.7% SiO₂ and 14.9% Na₂O), mass ratio 1:3. Tests were carried out in which the standard alkaline activator was replaced by the sodium silicate solution RF1.5-8 prepared in the previous reaction.

Proof tests with 5 different formulations were produced: geopolymer matrix with standard alkaline activator (Matrix): 50% metakaolin, 50% standard alkaline activator; matrix with silicate produced from IOT T1.5-8(L) (MSiIT): 50% metakaolin, 50% T1.5-8(L) solution; use of 50% IOT as a filler in the composition of the geopolymer and sodium silicate produced from the tailings as an activating solution (IOT50SiIT): 50% IOT, 25% metakaolin and 25% T1.5-8(L) solution; use of 25% IOT as a filler in the geopolymer composition (IOT25): 25% IOT, 37.5% metakaolin and 37.5% standard alkaline activator; use of 50% IOT as a filler in the geopolymer composition (IOT50): 50% IOT, 25% metakaolin and 25% standard alkaline activator.

For the preparation of the specimens, at first the solid precursors were mixed until homogenized, the alkaline activator was added to the solid mixture and stirred until its consistency was adequate to mold the specimens. The geopolymeric paste was added in small cylindrical molds (approximately 35 g each, 2 cm in diameter and 4 cm in length, Figure S1 (Supplementary Information (SI) section)) with the aid of a glass stick and vibration. The materials were demolded after 24 h of curing.

The geopolymers produced were analyzed by spectroscopy in the infrared region in a PerkinElmer spectrometer, Frontier Single Range MIR model (São Paulo, Brazil), in the attenuated total reflectance (ATR) module. The spectra were obtained in a spectral range from 4000 to 550 cm⁻¹, 16 scans and a resolution of 4 cm⁻¹. X-ray diffraction analyzes of the geopolymers were performed in a Philips-PANalytical diffractometer model PW3710 (Amsterdam, Netherlands), using Cu K α radiation and a graphite monochromator, range: 3 at 90° (2 θ), step 0.02° 2 θ time *per* count 3 s. SEM analyzes were performed on the same equipment and with the same procedures described for the materials previously. Tests of mechanical resistance to compression were made with the geopolymers produced. The tests were carried out in an Engetotus electric press (Contagem, Brazil) for a capacity of up to 100 tons.³¹

Results and Discussion

Sodium silicate synthesis

The IOT used in this work showed a chemical composition obtained by XRF analysis of ca. 71% SiO₂ and 23% Fe₂O₃, with small concentration of several other metals, as shown in Table 2.

Table 2. Analysis of mineral phases present in IOT by X-ray fluorescence (XRF)

| Mineral phase | Content / wt. % |
|--------------------------------|-----------------|
| SiO ₂ | 71 |
| Fe ₂ O ₃ | 23 |
| Al ₂ O ₃ | 3 |
| MgO | 2 |
| Cr ₂ O ₃ | 0.39 |
| SO ₃ | 0.18 |
| CaO | 0.04 |
| MnO | 0.01 |

In order to obtain a silicate solution, a hydrothermal route was performed with IOT mixed with NaOH solution in a closed system under pressure (autoclave) at 200 °C.

Two main parameters were evaluated: the influence of NaOH concentration (1:1.5 and 1:2.5 of Si:NaOH molar ratio) and reaction time (4 and 8 h). The solid fraction obtained was separated from the liquid by centrifugation and both were analyzed. The samples are named here on as for example T1.5-4, where 1.5 is the SiO₂:NaOH molar ratio and 4 is the reaction time 4 h.

Figure 1 shows the X-ray diffractograms of the solids obtained in the reactions of iron tailings with NaOH, and also of the IOT for comparison. The IOT diffractogram shows the presence of three main phases: quartz SiO₂ (JCDPS 46-1045), with higher intensity peaks, hematite Fe₂O₃ (JCDPS 33-664) and goethite FeOOH (JCDPS 81-463), with peaks of lower intensity. It is observed that the materials T1.5-4, T1.5-8 and T2.5-4 also present peaks related to hematite, quartz and goethite phases, but the intensity of the peaks related to the quartz phase is much lower in these samples than in the pure tailings, indicating a partial solubilization of quartz. In addition, when comparing the materials after 4 and 8 h reactions, a decrease in quartz intensity is noticeable, suggesting that reaction time also played an important role in the products formed. Last, for the T2.5-8 sample, only peaks referring to the hematite and goethite phases were observed, indicating that under these conditions there was the total solubilization or amorphization of the quartz.

In order to estimate the quartz solubilization extension, the ratios were calculated using the intensities of the most intense peaks from quartz and hematite phases, ca. 2θ at 26.50 and 33.10°, respectively. The values obtained are shown in the graph in Figure 1.

The crystallite size for the quartz phase was calculated using the Debye Scherrer equation (equation S1, SI section) and the results obtained were 204.1, 220.9, 214.9 and 238.3 Å for IOT, T1.5-4, T1.5-8 and T2.5-4, respectively. It is possible to observe that there was an increase in the crystallite size of the silica phase after the solubilization reaction. It is believed that NaOH reacts primarily with the more reactive silica, such as the one with the smallest crystallite size. The concentration of NaOH in the medium was a more important parameter for the increase of the particle size than the reaction time.

The IOT and the solids obtained in the reactions were analyzed by Mössbauer spectroscopy to characterize the iron phases present. Figure 2 presents the Mössbauer spectra obtained and Table S1 (SI section) presents the calculated hyperfine parameters and the proportions of the mineral phases containing iron for these samples. The Mössbauer spectra of the samples have two sextets. The sextets in red have hyperfine parameters consistent with hematite (isomeric displacement = 0.36 mm s⁻¹,

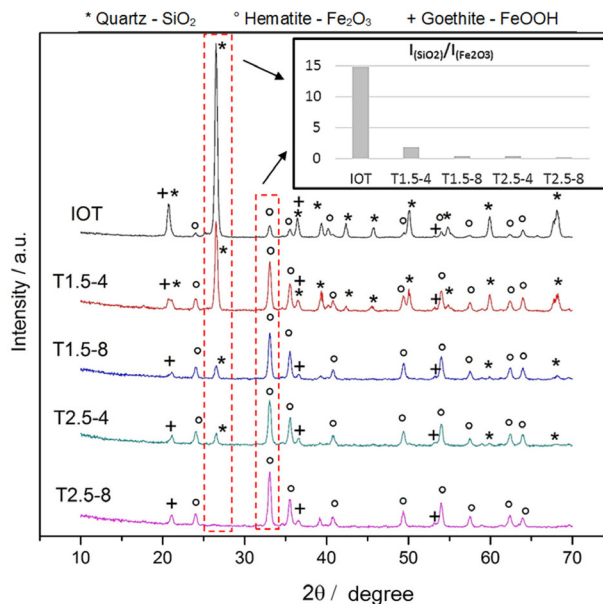


Figure 1. X-ray diffractograms of the solids obtained after hydrothermal reactions and pure IOT. Highlighted, the main peaks referring to the quartz ($2\theta = 26.50^\circ$) and hematite ($2\theta = 33.10^\circ$) phases and a graph with the $I_{\text{SiO}_2}/I_{\text{Fe}_2\text{O}_3}$ ratios.

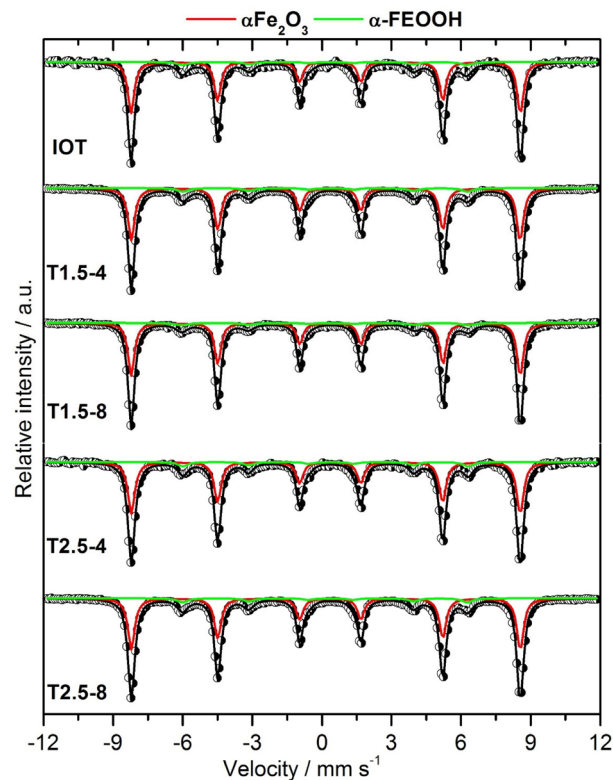


Figure 2. Mössbauer spectra of the solids obtained after hydrothermal reactions and pure IOT.

quadrupolar displacement = -0.19 mm s^{-1} and hyperfine field = 51.9 T), while the sextets in green can be attributed to goethite (isomeric displacement = 0.36 mm s^{-1} , quadrupolar displacement = -0.26 mm s^{-1} and hyperfine field = 38.0 T).^{32,33} The relative areas ranged from 83 to

88% for hematite and 12 to 17% for goethite, which shows that the iron phase present in greater quantity is hematite. These results indicate that there were no significant changes in the iron phases present in the tailings after treatment with NaOH.

SEM analyses (Figure 3) were performed to observe changes in the morphology of the solid products and IOT. From the obtained images, it can be observed that the materials are very heterogeneous and have particles of varying sizes. The mapping of the elements indicated the presence of silicon (yellow) and iron (purple) in the samples, in agreement with XRF and XRD analysis. It is observed that the IOT mapping shows the majority presence of silicon, while in the treated samples there are few regions with the presence of silicon and a majority presence of iron, which also corroborates the obtained results.

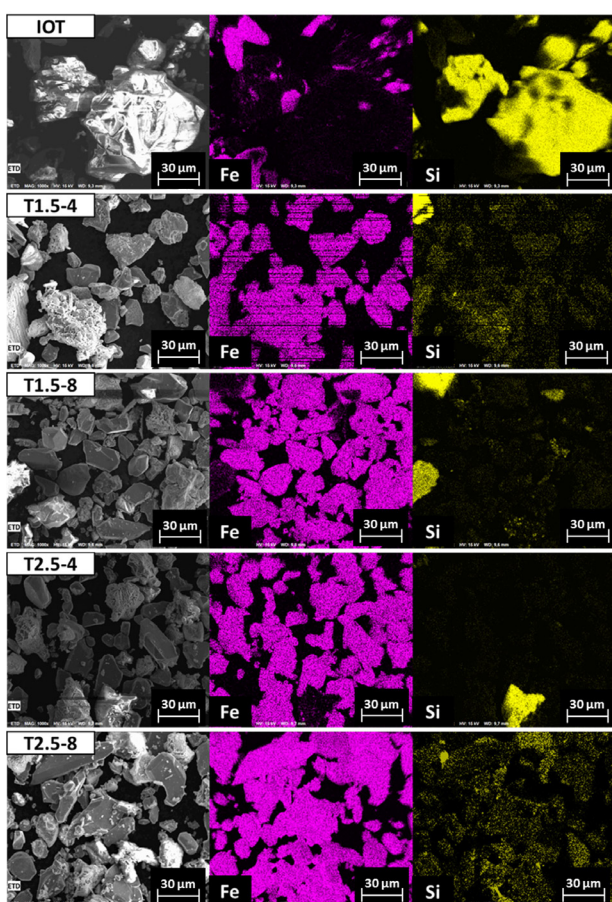


Figure 3. Scanning electron microscopy images and EDS mapping of solids obtained after hydrothermal reactions and pure IOT. The EDS mapping of iron is represented in purple and the silicon in yellow.

As mentioned before, the reaction had a solid and a liquid product. The sodium silicate solutions were analyzed by titration to determine the contents of SiO_2 and Na_2O . For materials T2.5-4 and T2.5-8, there was the formation of a precipitate of NaOH in the liquid fraction after a day

of rest, indicating a large excess of NaOH in the solution, therefore these materials were not analyzed by titration. The values obtained for materials T1.5-4 and T1.5-8 were ca. 19-20% Na_2O and 19-23% SiO_2 (see Table S2 in SI section). These results combined with XRD and EDS suggest that the majority of SiO_2 present in the IOT was solubilized. The liquid obtained for the material T1.5-8 was used for geopolymer synthesis. The solid material resulting from the reaction has the potential to be sold as a high value iron ore due to the high concentration of iron, estimated at 82% Fe_2O_3 .

Geopolymers synthesis

The main constituents in geopolymer formulation are silicate, NaOH, the Al source and a filler. The rate of polymer formation is influenced by many parameters, such as the curing temperature, water content, alkaline ratio, initial solids content, silicate and aluminate ratio, pH and the types of activators used. These parameters have substantial effects on the final properties of geopolymers.³⁴ Thus, the composition of the raw materials to be used must be well defined, as well as the quantities used in the mixtures. Therefore, the composition of the Al source (metakaolin) used was analyzed by X-ray fluorescence, and the results are shown in Table S3 (SI section).

The $\text{SiO}_2/\text{Al}_2\text{O}_3$ molar ratio has a great impact on the synthesis of geopolymers, as the amount of SiO_2 available directly influences the formation of polymeric Si–O–Al bonds.³⁴ Thus, the composition of alkaline activators is a critical parameter. The standard alkaline activator was previously prepared using a mass ratio 1:3 of 10 M sodium hydroxide solution and a commercial sodium silicate solution (32.7% SiO_2 and 14.9% Na_2O). The total contents of the alkaline activator calculated were 24.5% SiO_2 and 17.0% Na_2O . The sodium silicate solution obtained from the hydrothermal reaction of IOT with NaOH T1.5-8 showed contents of 22.6% SiO_2 and 19.3% Na_2O , which are close to those calculated for the standard activator solution. Thus, this solution was chosen to replace the alkaline activator in order to produce geopolymers.

For the preparation of the geopolymers specimens, the solid precursors were mixed until homogenized, the alkaline activator was added to the solid mixture and stirred until its consistency was adequate to mold the specimens. The geopolymeric paste was added in small cylindrical molds with the aid of a glass stick and vibration, and the materials were demolded after 24 h of curing. The geopolymers were produced and named according to the Table 3. The material named Matrix was made using commercial sodium silicate solution without addition of IOT as a filler for comparison with the other materials.

The specimens were demolded after a day of curing. In none of the specimens, cracks or bubbles were observed. Figure 4 shows the specimens produced after 7 days of curing.

Table 3. Geopolymers produced and formulations

| Nomenclature | Silicate solution / wt. % | Silicate solution source | Metakaolin / wt. % | IOT in the geopolymer / wt. % |
|--------------|---------------------------|--------------------------|--------------------|-------------------------------|
| Matrix | 50 | commercial | 50 | – |
| MSiIT | 50 | IOT silicate | 50 | – |
| IOT25 | 37.5 | commercial | 37.5 | 25 |
| IOT50 | 25 | commercial | 25 | 50 |
| IOT50SiIT | 25 | IOT silicate | 25 | 50 |

IOT: iron ore tailings.

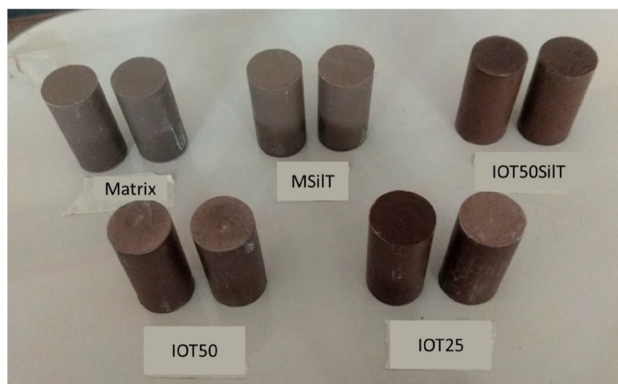


Figure 4. Geopolymers produced with different compositions.

The materials were analyzed by X-ray diffraction to verify the crystalline phases. Figure 5 shows the X-ray diffractograms obtained for metakaolinite and for the geopolymers produced. The iron tailings X-ray diffractogram has already been discussed previously. The presence of two phases can be observed in the metakaolinite diffractogram (MK): quartz SiO_2 (JCDPS 46-1045), with higher intensity peaks, and kaolinite $\text{Al}_2(\text{Si}_2\text{O}_5)(\text{OH})_4$ (JCDPS 80-885), with peaks of lesser intensity. It is known that metakaolinite has a typically amorphous structure and, therefore, a protuberance is observed in the region between 20 and 40°, referring to the amorphous phases.³⁵ The presence of peaks referring to the kaolinite phase indicates that the metakaolinite has kaolinite in its composition that has not reacted in the metakaolinite production process.

In the diffractograms of the geopolymers Matrix and MSiIT, the peaks referring to quartz are observed, and the formation of a protuberance between 20 and 40°, characteristic of the formation of gel in geopolymers, is also observed.³⁵ In the diffractogram of geopolymers IOT25, IOT50 and IOT50SiIT, it is observed the presence of

peaks referring to quartz, with greater intensity than in the previous materials, and hematite Fe_2O_3 (JCDPS 33-664). For these materials the bulge between 20 and 40° is no longer observed. These results are expected since those materials are predominantly crystalline due to the presence of IOT. It is observed that for the materials IOT50 and IOT50SiIT the peaks referring to the crystalline phases are more intense, since these materials have a greater amount of tailing in their composition.

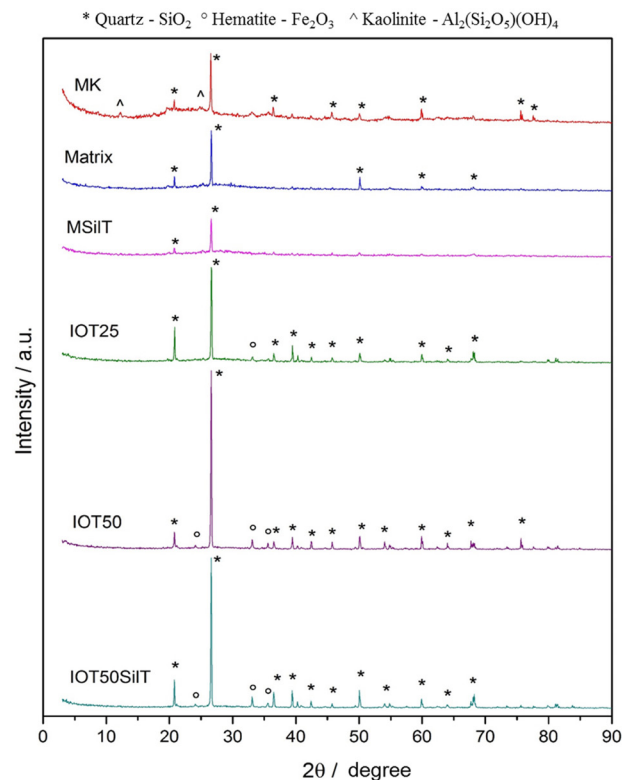


Figure 5. X-ray diffractograms of the metakaolinite and the geopolymers produced.

Iron ore tailings, metakaolinite and geopolymers produced were analyzed by infrared spectroscopy (Figure 6). In all spectra, it is observed the presence of a band at approximately 1000 cm^{-1} , referring to the stretching of the Si–O–Si and Al–O–Si tetrahedral bonds. As highlighted by the dotted line, for the tailings and metakaolinite, the band is closer to 1032 cm^{-1} , so the geopolymeric synthesis caused a displacement of this band to regions with lower wavenumbers. This shift was also observed by other researchers in the synthesis of geopolymers, who attributed this phenomenon to the change in the coordination of aluminum and the change in the chemical environment of the atoms due to geopolymerization.^{7,36}

In the metakaolinite spectrum, bands with small intensity at approximately 3600 cm^{-1} related to stretches of Al–O–H bonds of kaolinite are observed.³⁷ The presence

of these bands indicates that kaolinite did not completely react in the process of obtaining metakaolinite, which corroborates what was observed in the XRD analysis of metakaolinite.

In the spectra of all geopolymers, bands are observed at approximately 3400 and 1650 cm^{-1} referring to the presence of water adsorbed on the materials.³⁸ Also, a band observed at approximately 1450 cm^{-1} was attributed by other researchers as the presence of C–O stretches from carbonates, indicating a carbonation process (known as efflorescence) in the produced geopolymers.^{39,40}

In the spectra of metakaolinite and iron tailings, bands around 750 cm^{-1} are observed, which correspond to the Si–O deformation of quartz present in both materials.⁴¹ For the produced geopolymers that present the tailings as filler, IOT25, IOT50 and IOT50SiIT, these bands are also observed due to the more significant presence of quartz in the materials. For the others, these bands are not observed. The characteristic vibrational bands of Fe–O bonds from iron oxides are at wavelengths from 430 to 680 cm^{-1} , so they could not be clearly observed in the obtained spectrum.⁴²

Precursor materials and the produced geopolymers were also analyzed by SEM-EDS. Figures 7 and 8 show the images obtained for the Matrix and IOT50 geopolymers, the images of the other materials are in the SI section (Figures S2, S3 and S4). In all materials, there is a very homogeneous structure, but without a defined shape, which is characteristic of amorphous materials. In all materials, elements mapping indicates the majority presence of sodium, aluminum, silicon and iron, indicated by the colors red, green, yellow and lilac, respectively.

In the element mapping of the geopolymer Matrix, it is observed the presence of some points of heterogeneity, as highlighted in the image, that the mapping indicated greater

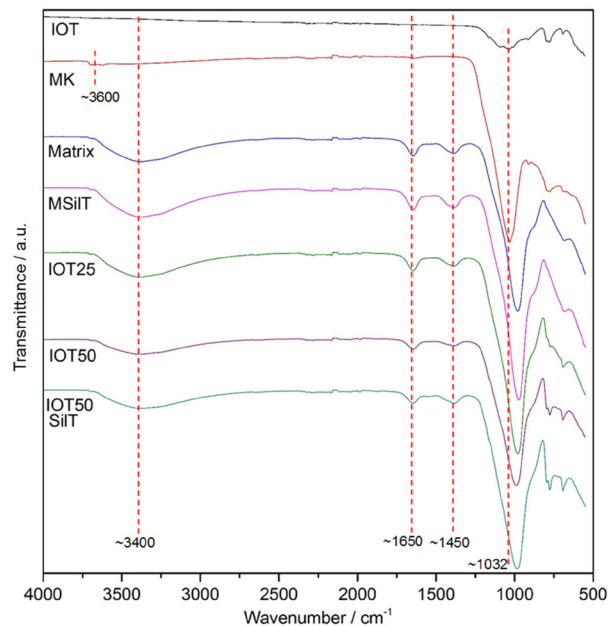


Figure 6. FTIR (ATR) spectra of the solids obtained after hydrothermal reactions and pure IOT.

intensity of aluminum and absence of sodium. This possibly indicates the presence of kaolinite from metakaolin that did not react in the geopolymerization process. The XRD and infrared results showed the presence of unreacted kaolinite in metakaolinite and, due to its crystallinity, kaolinite is much less reactive. Points where silicon predominates are also observed, possibly due to the quartz that is also present in the metakaolinite and does not react in the geopolymerization process.

In the elements mapping of geopolymers that present iron tailings as a filler, it is observed the presence of several isolated particles indicating iron and silicon, as highlighted in the image. This indicates that the hematite

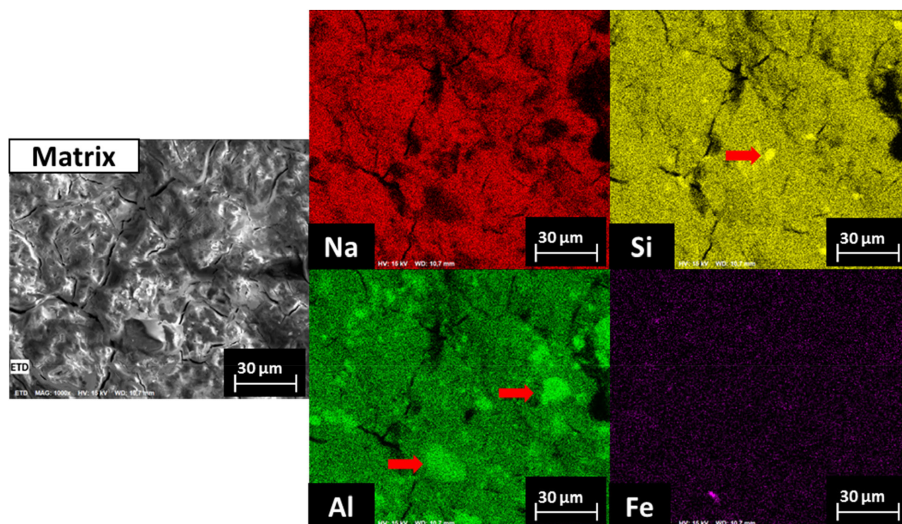


Figure 7. Scanning electron microscopy images and EDS mapping of Matrix.

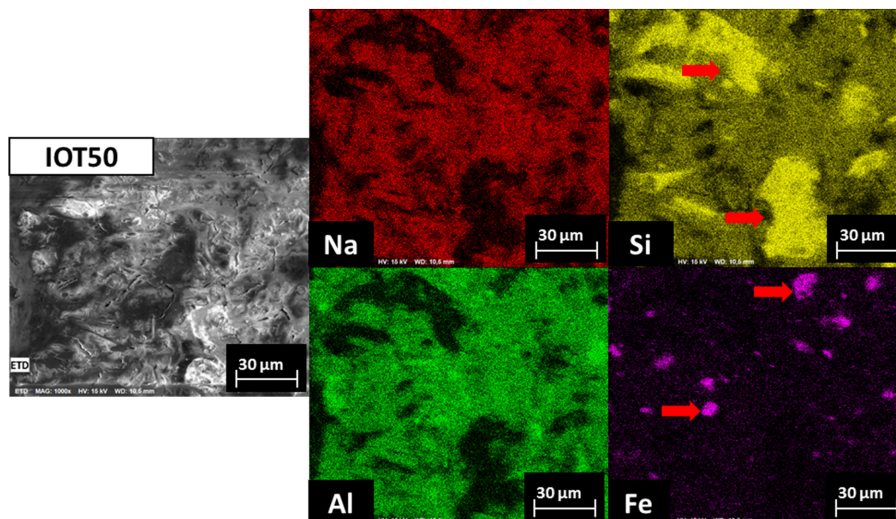


Figure 8. Scanning electron microscopy images and EDS mapping of IOT50.

and quartz present in the tailings kept their phases after geopolymerization, which agrees with the role of filler.

After 7 days of curing, tests of mechanical resistance to compression were performed with the specimens. The obtained results are shown in Figure 9. The results obtained for the geopolymer prepared with standard activator solution (Matrix) and with the produced sodium silicate solution (MSiIT) are very similar, which indicates that the produced silicate solution is efficient for use in the production of geopolymers. The materials prepared with IOT as fillers also showed very similar values to the Matrix, indicating that the use of these tailings as fillers did not affect the strength properties of the geopolymer.

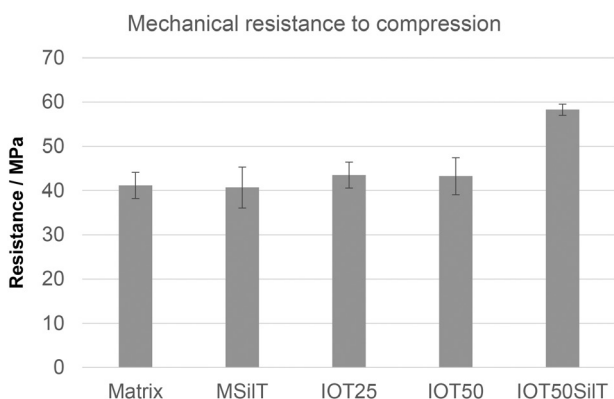


Figure 9. Values of mechanical resistance to compression of the produced geopolymers.

The use of 50% of IOT and sodium silicate, both produced from the tailings, led to considerably higher resistance results than the Matrix. It is not known what may have led to this increase in resistance, since the use of 50% of tailings and standard activating solution and only replacing the standard activating solution with the

silicate produced in the conventional Matrix did not affect the resistance results, so it cannot attribute this increase to one of the modifications separately.

Considering that conventional concrete bodies are tested only after 28 days of curing and have values of mechanical resistance to compression around 25 MPa,⁴³ all the results for the geopolymers produced in this work are promising, since the mechanical resistance to compression is superior and requires only 7 days of cure. Moreover, these values are also very positive compared to other geopolymers in the literature.¹⁸ Studies¹⁸ have been found in the literature using red mud, fly ash and blast furnace slag in the composition of geopolymers, and the compressive strengths of these materials are extremely variable, ranging from 5.5 to 49.2 MPa, but most are in the range of 5-20 MPa.¹⁸

Conclusions

In this work, sodium silicate was produced from iron mining tailings, which was applied in the production of geopolymers. Initially, reactions of the IOT with NaOH were carried out to obtain a solution of sodium silicate and iron oxide. Under the reaction conditions of 1:2.5 of IOT:NaOH and a reaction time of 8 h, the total solubilization of the silica from the IOT was possible. In addition, a sodium silicate solution was produced with SiO₂ and Na₂O contents very close to an activator solution usually used for the production of geopolymers, so this produced solution was used for this application. Geopolymers with different compositions were produced using IOT as filler and the sodium silicate solution produced from IOT as alkaline activator. Compressive strength tests were performed on the geopolymers produced and the results obtained were very positive, ranging from 40.72 to 58.28 MPa.

Supplementary Information

Supplementary data are available free of charge at <http://jbcbs.sbg.org.br> as PDF file.

Acknowledgments

The authors acknowledge the UFMG Microscopy Center for the images and the support of CNPQ, INCT Midas, CAPES and FAPEMIG.

Author Contributions

Caroline D. Prates was responsible for conceptualization, methodology, formal analysis, writing original draft, visualization; Athos S. Lima for investigation; Igor C. Ferreira for investigation; Fabiano G. F. de Paula for investigation; Paula S. Pinto for investigation; José D. Ardisson for investigation; Rochel M. Lago for conceptualization, resources, supervision; Ana Paula C. Teixeira for conceptualization, methodology, resources, visualization, supervision.

References

- da Silva, A. P. M.; Viana, J. P.; Cavalcante, A. L. B.; *Diagnóstico dos Resíduos Sólidos da Atividade de Mineração de Substâncias Não Energéticas*; IPEA: Brasília, 2012. [Link] accessed on November 24, 2022
- de Carvalho, P. S. L.; Mesquita, P. P. D.; Regis, R. D. D.; Meirellis, T. L.; *Sustentabilidade Socioambiental da Mineração*; BNDES, 2018. [Link] accessed on November 24, 2022
- de Andrade, L. C. R.; *Caracterização de Rejeitos de Mineração de Ferro, in natura e Segregados, para Aplicação como Material de Construção Civil*; PhD Thesis, Universidade Federal de Viçosa, Viçosa, Brazil, 2014. [Crossref]
- Prates, C. D.; *Utilização de um Rejeito de Minério de Ferro no Desenvolvimento de um Catalisador Heterogêneo Ácido para a Síntese de Biodiesel*; MSc Dissertation, Universidade Federal de Minas Gerais, Belo Horizonte, Brazil, 2018. [Link] accessed in November 2022
- Carmignano, O. R.; Vieira, S. S.; Teixeira, A. P. C.; Lameiras, F. S.; Brandão, P. R. G.; Lago, R. M.; *J. Braz. Chem. Soc.* **2021**, *32*, 1895. [Crossref]
- Bicalho, H. A.; Rios, R. D. F.; Binatti, I.; Ardisson, J. D.; Howarth, A. J.; Lago, R. M.; Teixeira, A. P. C.; *J. Hazard. Mater.* **2020**, *400*, 123310. [Crossref]
- Figueiredo, R. A. M.; Brandão, P. R. G.; Soutsos, M.; Henriques, A. B.; Fourie, A.; Mazzinghy, D. B.; *Mater. Lett.* **2021**, *288*, 129333. [Crossref]
- Prates, C. D.; Ballotin, F. C.; Limborço, H.; Ardisson, J. D.; Lago, R. M.; Teixeira, A. P. C.; *Appl. Catal., A* **2020**, *600*, 117624. [Crossref]
- Silva, R. C. F.; *Utilização de um Rejeito de Minério de Ferro para a Produção de Nanomateriais de Carbono em Leito Fluidizado e Aplicação desses Materiais na Adsorção de um Contaminante Emergente*; MSc Dissertation, Universidade Federal de Minas Gerais, Belo Horizonte, Brazil, 2018. [Link] accessed in November 2022
- Luciano, V. A.; de Paula, F. G.; Pinto, P. S.; Prates, C. D.; Pereira, R. C. G.; Ardisson, J. D.; Rosmaninho, M. G.; Teixeira, A. P. C.; *Fuel* **2022**, *310*, 122290. [Crossref]
- Zucheratte, A. C. V.; Freire, C. B.; Lameiras, F. S.; *Constr. Build. Mater.* **2017**, *151*, 859. [Crossref]
- da Silva, F. L.; Araújo, F. G. S.; Teixeira, M. P.; Gomes, R. C.; von Krüger, F. L.; *Ceram. Int.* **2014**, *40*, 16085. [Crossref]
- Pinto, A. T.; *Introdução ao Estudo dos Geopolímeros*; Universidade De Trás-Os-Montes E Alto Douro, Vila Real, Portugal, 2006. [Link] accessed in November 2022
- Costa, A. F. M.; *Utilização de Geopolímeros para Proteção de Betão: Resistência a Altas Temperaturas*; MSc Dissertation, Universidade do Minho, Braga, Portugal, 2012. [Link] accessed in November 2022
- Cunha, M. J. F. M.; *Durabilidade de Geopolímeros Monofásicos*; MSc Dissertation, Universidade do Minho, Braga, Portugal, 2013. [Link] accessed in November 2022
- Hu, W.; Nie, Q.; Huang, B.; Shu, X.; He, Q.; *J. Cleaner Prod.* **2018**, *186*, 799. [Crossref]
- Ye, N.; Yang, J.; Ke, X.; Zhu, J.; Li, Y.; Xiang, C.; Wang, H.; Li, L.; Xiao, B.; *J. Am. Ceram. Soc.* **2014**, *97*, 1652. [Crossref]
- Hairi, S. N. M.; Jameson, G. N. L.; Rogers, J. J.; MacKenzie, K. J. D.; *J. Mater. Sci.* **2015**, *50*, 7713. [Crossref]
- Das, S. K.; Kumar, S.; Ramachandrarao, P.; *Waste Manage.* **2000**, *20*, 725. [Crossref]
- Duan, P.; Yan, C.; Zhou, W.; Ren, D.; *Ceram. Int.* **2016**, *42*, 13507. [Crossref]
- Kuraniche, F. A.; Shukla, S. K.; Habibi, D.; *Int. J. Min., Reclam. Environ.* **2016**, *30*, 92. [Crossref]
- Foletto, E. L.; Gratieri, E.; de Oliveira, L. H.; Jahn, S. L.; *Mater. Res.* **2006**, *9*, 335. [Crossref]
- Deabriges, J.; *US pat. 4336235A*, **1982**. [Link] accessed on November 24, 2022
- Metzger, J.; Lecouls, H.; Colombe, P.; Wojcik, J.; *US pat. 4520001A*, **1985**. [Link] accessed on November 24, 2022
- Christophliemk, P.; Novotny, R.; Von Laufenberg, J.; *US pat. 4770866A*, **1988**. [Link] accessed on November 24, 2022
- Haase, R.; Hunger, V.; Lenz, A.; *US pat. 3984526A*, **1976**. [Link] accessed on November 24, 2022
- Blencoe, J. G.; Palmer, D. A.; Anovitz, L. M.; Beard, J. S.; *US pat. 10632418B2*, **2012**. [Link] accessed on November 24, 2022
- Vinai, R.; Soutsos, M.; *Cem. Concr. Res.* **2019**, *116*, 45. [Crossref]

29. Brand, R. A.; *Normos-90 Laboratorium für Angewandte Physik*; Universität Duisburg: Duisburg, Germany, 1999.
30. *Standard Methods for the Examination of Water and Wastewater*; Rice, E. W.; Baird, R. B.; Eaton, A. D.; Clesceri, L. S., eds.; APHA: Washington, D.C., USA, 1995.
31. Ferreira, I. C.; Galéry, R.; Henriques, A. B.; Teixeira, A. P. C.; Prates, C. D.; Lima, A. S.; Souza Filho, I. R.; *J. Mater. Res. Technol.* **2022**, *18*, 4194. [Crossref]
32. Stevens, J. G.; Khasanov, A. M.; Miller, J. W.; Pollak, H.; Li, Z.; *Mossbauer Mineral Handbook*; Mossbauer Effect Data Center: North Carolina, USA, 1998.
33. Vandenberghe, R. E.; Barrero, C. A.; da Costa, G. M.; Van San, E.; de Grave, E.; *Hyperfine Interact.* **2000**, *126*, 247. [Crossref]
34. dos Santos, F. A.: *Estudo da Variação da Relação SiO₂/Al₂O₃ na Produção de Geopolímeros para Imobilizar Contaminantes*; MSc Dissertation, Universidade Federal de Pernambuco, Pernambuco, Brazil, 2017. [Crossref]
35. Freire, A. L.; Moura-Nickel, C. D.; Scaratti, G.; de Rossi, A.; Araújo, M. H.; de Noni Jr., A.; Rodrigues, A. E.; Castellón, E. R.; Moreira, R. F. P. M.; *J. Cleaner Prod.* **2020**, *273*, 122917. [Crossref]
36. Somna, K.; Jaturapitakkul, C.; Kajitvichyanukul, P.; Chindaprasirt, P.; *Fuel* **2011**, *90*, 2118. [Crossref]
37. Madejová, J.; *Vib. Spectrosc.* **2003**, *31*, 1. [Crossref]
38. Tang, N.; Deng, Z.; Dai, J.-G.; Yang, K.; Chen, C.; Wang, Q.; *J. Cleaner Prod.* **2018**, *192*, 906. [Crossref]
39. Bouguermouh, K.; Bouzidi, N.; Mahtout, L.; Pérez-Villarejo, L.; Martínez-Cartas, M. L.; *J. Non-Cryst. Solids* **2017**, *463*, 128. [Crossref]
40. Li, S.; Huang, X.; Muhammad, F.; Yu, L.; Xia, M.; Zhao, J.; Jiao, B.; Shiau, Y.; Li, D.; *RSC Adv.* **2018**, *8*, 32956. [Crossref]
41. Louati, S.; Baklouti, S.; Samet, B.; *Adv. Mater. Sci. Eng.* **2016**, *2016*, ID 2359759. [Crossref]
42. Kaur, K.; Jain, P.; Sobti, A.; Toor, A. P.; *Green Process. Synth.* **2016**, *5*, 93. [Crossref]
43. Mehta, P. K.; Gjörv, O. E.; *Cem. Concr. Res.* **1982**, *12*, 587. [Crossref]

Submitted: July 10, 2022

Published online: December 2, 2022

